IEEE Access
Multidisciplinary | Rapid Review | Open Access Journal

IEEE PHOTONICS SOCIETY SECTION

Received 22 April 2024, accepted 17 May 2024, date of publication 23 May 2024, date of current version 4 June 2024.

Digital Object Identifier 10.1109/ACCESS.2024.3404632

RESEARCH ARTICLE

On the Effect of Air Bubbles-Induced Scattering on Turbid Waters: An Experimental UOWC Channel Modeling Approach

PEDRO SALCEDO-SERRANO, CARLOS GÓMEZ-GARCÍA, JACQUELINE IAMAGUTI-DEBESSA, RUBÉN BOLUDA-RUIZ, JOSÉ MARÍA GARRIDO-BALSELLS, BEATRIZ CASTILLO-VÁZQUEZ, ANTONIO PUERTA-NOTARIO, AND ANTONIO GARCÍA-ZAMBRANA

Telecommunication Research Institute (TELMA), University of Málaga, 29010 Málaga, Spain

Corresponding author: Pedro Salcedo-Serrano (pss@ic.uma.es)

This work was supported in part by the Spanish Ministerio de Ciencia, Innovación y Universidades under Grant FPU22/02183; in part by the project from the Spanish MICINN under Grant PID2019-107792GB-I00; and in part by the Plan Andaluz de Investigación, Desarrollo e Innovación (PAIDI) 2021, under Grant P21_00390.

ABSTRACT The influence of the oceanic medium on the underwater optical wireless communication (UOWC) highlights the need for an accurate mathematical channel characterization that models the properties of realistic oceanic environments, significantly optimizing the development of practical UOWC system designs. However, a need remains to provide a deeper insight into the behavior of air bubbles in turbid waters. This article presents an analysis and a statistical characterization of the received optical power fluctuations when considering different air bubble sizes and levels of particle-induced scattering. Experimental measurements were conducted in a water tank, manipulating water turbidity levels by dissolving a commercial antacid. Afterward, some evaluation metrics, such as the scintillation index, the average outage duration, and the coherence time, are calculated to provide an analytical framework of the air bubbles-induced fading in turbid environments. Additionally, the statistical behavior of small and large air bubbles are analytically described through the generalized Gamma distribution and a mixture of two generalized Gamma distributions, respectively, and validated with a coefficient of determination above 0.95 for all the considered turbid waters. Results demonstrate that water turbidity dramatically affects the stochastic behavior of the underwater channel in the presence of air bubbles, resulting in a significant reduction in light blockage due to the collection of scattered photons. As a result, the scintillation index and the average outage duration are noticeably reduced for more turbid water.

INDEX TERMS Air bubbles, fading channel, oceanic turbulence, scattering, turbid water, underwater optical wireless communication, underwater free-space optical.

I. INTRODUCTION

In recent years, a growing interest in marine exploration has motivated the development of new wireless systems that support high speed communications, particularly in real-time applications. Underwater optical wireless communications (UOWC) systems have emerged as a viable candidate for these bandwidth-hungry and delay-sensitive applications thanks to its broad bandwidth and high data rate with low latency [1], [2], [3]. However, the major drawback of deploying UOWC links is the inherent impairments of the underwater optical channel, such as the absorption and scattering processes due to dissolved and in-suspension particles, which noticeably reduce the link span and the maximum achievable data rate. The severity of these constraints varies significantly depending on the underwater environments, commonly classified according to their turbidity as clear ocean, coastal and harbor waters, as well as the different Jerlov water types [4], [5], [6], [7]. In addition to these effects, the transmitted optical beam is affected by random

The associate editor coordinating the review of this manuscript and approving it for publication was Leo Spiekman.

fluctuations in the irradiance as a result of small variations in temperature and salinity concentrations, commonly referred to as oceanic turbulence [8], [9]. Likewise, the presence of air bubbles also causes random fluctuations in the refractive index owe to the interface between water and air bubbles [10]. Extensive research has been conducted on the origin of air bubbles in underwater medium, including the breaking waves, cavitation caused by marine vehicle propellers, phytoplankton photosynthesis, or zooplankton respiration [11], [12], [13], [14]. However, the lack of realistic experimental studies in UOWC channel modeling under air bubbles has obstructed the development of accurate channel models, impeding an optimal design of optical transceivers. Despite the complexities of conducting measurements in open oceans, cost-effective results can be obtained under controlled laboratory conditions.

In contrast to the vast literature on oceanic turbulence, there have been few investigations into the statistical behavior of the bubbles-induced scattering in UOWC channels [15], [16], [17], [18], [19], [20] (and references therein). In [15], an experimental UOWC system is evaluated in terms of the bit error rate (BER) under bubbles-induced scattering. The authors highlight that the UOWC system design can be adapted in order to properly mitigate the UOWC channel effects considering the density and size of air bubbles. In [16], a statistical characterization of the intensity fluctuations is experimentally analyzed under air bubbles and oceanic turbulence. In that article, the authors concluded that the generalized Gamma and the Weibull probability density functions (PDF) are the most suitable for fitting the experimental data. In [17], a unified statistical model under temperature gradients in the presence of air bubbles for fresh and salty waters is proposed, utilizing a mixture Exponential–generalized Gamma distribution. However, the derived UOWC system performance expressions have not been validated through experimental results. In [18], it is demonstrated that the BER performance of a UOWC system depends on the density and the size of air bubbles. In [19], the authors proposed a statistical model that describes the size and the horizontal distribution of air bubbles to calculate the combined obstruction of all generated air bubbles via simulation. Regarding the combined impact of air bubbles and marine particles, as far as we know, only one study in terms of simulation has been published [20]. In this piece of work, they calculated the increase in the delay spread of the channel due to air bubbles in different types of water.

As mentioned above, the air bubbles represent one of the main inconveniences when deploying practical UOWC systems. Although some theoretical and experimental insights have been gained about the impact of air bubbles on UOWC links, this has not been considered in isolation yet in channel modeling based on experimental measurements, since it has been always analyzed along with other turbulent phenomena such as temperature gradients that obscured its analysis. Furthermore, to our knowledge, there is no research on thoroughly analyzing the effect of the bubbles-induced fluctuations and its changing nature with the water turbidity. This is quite remarkable since the generation of air bubbles is directly related with some of important scattering agents such as phytoplankton and zooplankton [13], [14]. This will be critical for the design of the next UOWC systems generation, because significant underwater activities such as oceanographic observation, underwater environmental monitoring, or submerged infrastructure inspection are conducted in turbid water environments. It is noteworthy that current commercial UOWC systems such as the Sonardyne BlueComm 200 and the LUMA X solely offer high transmission speeds in clear water environments [21], [22]. Therefore, it is crucial first to establish a UOWC channel model that accurately characterizes the effects of the underwater environment across all types of water types, especially in turbid water in the presence of air bubbles, for which the scientific community has not yet developed high-speed UOWC systems tailored to activities mentioned above. In addition, conducting only a statistical model may not offer sufficient information for overall system design and configuration, particularly in adaptive transmission schemes. In such cases, measuring the coherence time and the average outage duration (AOD) becomes essential for adequately selecting the transmission symbol rate.

In this paper, we analyze and statistically model, for the first time, the impact of the water turbidity on the received optical power fluctuations due to air bubbles. Unlike previous papers which only use tap or salty water [16], [17], [18], [19], we modify the particle-induced scattering, i.e., the water turbidity, with a commercial antacid solution. Additionally, experiments are conducted for different air bubble sizes, which helps to extend the existing knowledge about the impact of scattering in realistic underwater environments. On the one hand, air bubble diameters range from approximately 1 mm for small bubbles to approximately 1 cm for large bubbles. On the other hand, the range of water turbidity levels in the emulated environments covers Jerlov IB to Jerlov 5C water types. For that, several evaluation metrics are obtained from the experimental measurements. These metrics provide a theoretical framework to analytically study the stochastic behavior of air bubbles-induced fading under different UOWC scenarios. Thus, the main contributions of this study are summarized as follows:

- We develop a UOWC experimental setup capable of emulating different underwater environments in terms of water turbidity with a commercial antacid. The generation of realistic columns of air bubbles with different sizes and marine currents is controlled by employing an air pump and two brushless motors with propellers.
- We analyze the losses, the received optical power fluctuations and the optical wavefront distortions due to small and large air bubbles through the scintillation index, the average outage duration, the coherence time, and the received footprint.

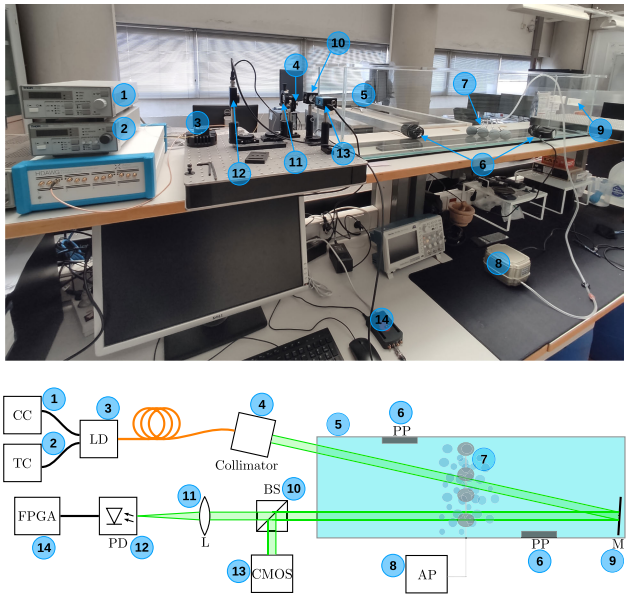

FIGURE 1. Experimental setup. (1) Current controller (CC). (2) Temperature controller (TC). (3) Pigtailed laser diode mount. (4) Fiber Collimator. (5) Water tank. (6) Propeller pump (PP). (7) Diffusers. (8) Air pump (AP). (9) Dielectric mirror. (10) Beamsplitter (BS). (11) Plano-convex lens (L). (12) Photodetector (PD). (13) Camera CMOS. (14) RedPitaya STEMlab.

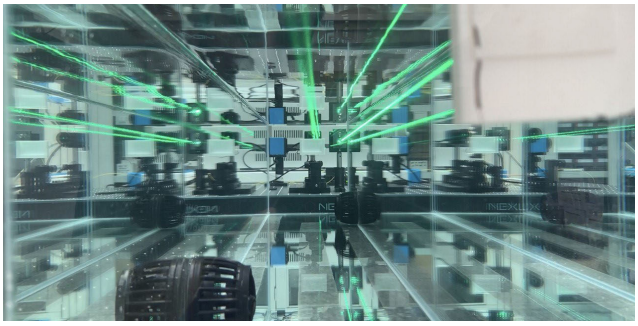

(a) Tap water

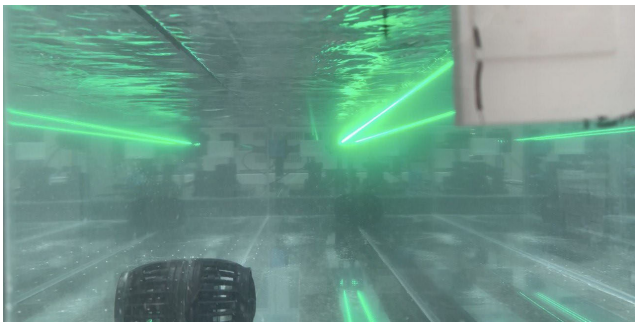

(b) Tap water with 7.3 mg/L of Maalox antacid

FIGURE 2. A green laser beam propagating through the water tank filled with tap water (a) with no antacid, and (b) with 7.3 mg/L of Maalox antacid.

- We propose and validate experimentally the generalized Gamma and a mixture of two generalized Gamma distributions in order to analytically model the statistical behavior of small and large air bubbles under several levels of scattering. These distributions allow to describe accurately bubbles-induced fluctuations with a goodness of fit in terms of the coefficient of determination above 0.95 for all the considered turbid waters.
- The experimental results show that bubbles-induced fluctuations are highly influenced by particle-induced scattering, resulting in a significant reduction in light obstruction due to the capture of scattered photons. Our data analysis reports for the first time a decrease in both the scintillation index and the average outage duration under more turbid water conditions.

This novel approach provides more accurate knowledge about the joint effect of ocean impairments and the degradation of UOWC systems in realistic and natural waters. The modeling of the channel encompasses an advancement of the design of high-quality and long-range UOWC transceivers specifically adapted to turbid environments.

The following sections are organized as follows: Section II describes the experimental setup and the measurement procedure in greater detail. Section III introduces the evaluation metrics used to characterize the air bubbles-induced fluctuations. Section IV presents the results of the channel measurements, along with the probability distribution fitting and data analysis. Finally, Section V sums up the concluding remarks of the article.

II. EXPERIMENTAL SETUP

In this section, the conducted experiment is described in greater detail, as well as how the measurements were performed. For illustration purposes, the experimental configuration of the UOWC system is depicted in Fig. 1.

A. UNDERWATER OPTICAL CHANNEL

The UOWC channel is emulated by a rectangular glass tank of $1.5 \times 0.2 \times 0.3$ m filled with tap water. The water tank is filled with 60 liters of tap water, resulting in a water height within the tank of 0.22 m.

The turbidity of water is modified by adding Maalox, a commercial antacid commonly used to simulate different types of marine environments due to the similarity of its volume scattering function to those obtained from realistic oceanic water samples [23], [24]. In order to guarantee the reproducibility in the turbidity levels, the amount of Maalox used in each experiment is accurately determined using a precision scale with resolution of 0.01 g. By way of example, Fig. 2 visually shows the impact of the antacid solution in terms of visibility in the water tank with 7.3 mg/L of Maalox dissolved in tap water, which in 60 liters of water is an amount of 0.44 g of Maalox.

Furthermore, a broadband dielectric mirror (Thorlabs, BBSQ2-E02) positioned on the side of the water tank is employed to extend the distance of the UOWC link.

B. AIR BUBBLES-INDUCED SCATTERING GENERATION

Regarding air bubbles characteristics, two key aspects are considered. Firstly, the density of air bubbles, or bubbles

population, is controlled by manipulating the airflow rate of an air pump with 4 air outlets. The air pump employed in this experiment has a maximum capacity of 16 L/min. To manually regulate the airflow, we use the flow regulator valves, which control each air outlet. Secondly, the size of the air bubbles is determined by 4 porous stones connected to each air outlet, acting as an air diffuser. To produce larger bubbles, these porous stones are removed from the air outlet. Because of the heterogeneity of the porous stones, the diameter of small air bubbles ranges from 1 to 4 mm. Conversely, large bubbles measure approximately 1 cm. The two considered density levels of air bubbles as well as both sizes of air bubbles, are shown in Fig. 3. It is important to note that the diameter measurements were conducted using digital image processing techniques. Photographic images of the bubbles with a resolution of 4032 × 3024 pixels taken at a distance of 5 cm were acquired during experiments and analyzed using software such as GIMP to determine their diameter in pixels. In order to translate the pixel measurements into physical distances, a reference distance between identifiable landmarks within the image was necessary, which in this study was determined as the distance of the metal pipe connected to the experimental setup. The diversity of bubble sizes presented here represents the different sources of air bubbles in marine environments, such as propeller cavitation and breaking wind waves. At the same time, the interactions among bubbles and with propellers lead to a random division and merging of bubbles. As a result, this process promotes increased diversity in the bubble size and shape across the medium. This emulation captures the imperfections and variations in bubbles characteristic of realistic underwater environments with natural air bubbles sources. The air outlets are positioned to simulate realistic clusters of air bubbles that tend towards the surface in the form of column, typically generated by biological processes of marine organisms. Furthermore, the bubble column is randomly distributed throughout the water tank using two propeller pumps, or brushless motors, which also emulate natural wind-generated currents.

C. TRANSMITTER AND RECEIVER SETUP

At the transmitter side, a 520 nm laser diode (Thorlabs, LP520-SF15) is used with a collimator lens adapted to free space. The laser diode mount includes a temperature controller (Thorlabs, TED200C) and a current controller (Thorlabs, LDC205C) to set the current and the temperature during the experiment to 90 mA and 25 °C, respectively. At the receiver side, a 2.5 mm convergent lens focused into a silicon photodetector (Thorlabs, PDA10A2) collects the received light after passing through the water tank. The PDA10A2 photodetector includes a transimpedance amplifier with gain of $G = 10$ kV/A. The output electrical signal from the photodetector is acquired by a development board Red Pitaya STEMlab, which is supported by a ARM Cortex-A9 and a Field Programmable Gate Array (FPGA) Xilinx Zynq 7010 [25]. Simultaneously, a high resolution camera (The Imaging Source, DFK 38UX253) with a CMOS image sensor (Sony, Pregius IMX253) collects the received footprint after passing through a beamsplitter.

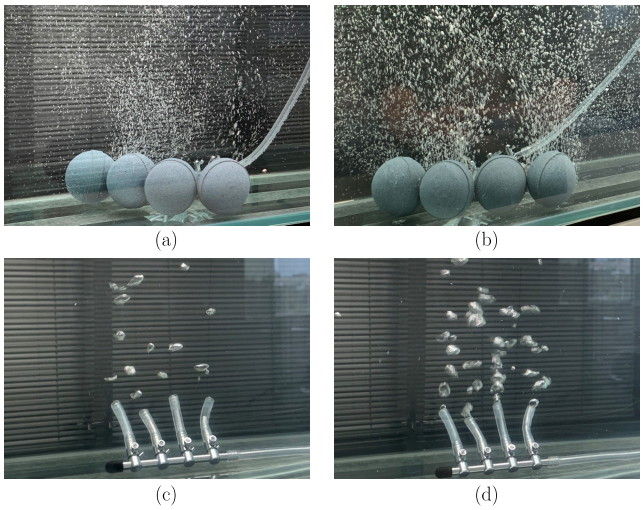

FIGURE 3. Proposed air bubbles scenarios: (a) small bubbles with low density (b) small bubbles with high density, (c) large bubbles with low density, and (d) large bubbles with high density.

III. EVALUATION METRICS

In this section, we define the evaluation metrics used to characterize the underwater optical channel and the received optical power fluctuations. In addition to the well-known parameters such as the attenuation coefficient of the water, and the scintillation index of the irradiance fluctuations, other key parameters are also measured with the goal of providing better understanding of the behavior of air bubbles-induced scattering fading. Specifically, we also characterize the coherence time of the fluctuations due to air bubbles and the average outage duration.

A. ATTENUATION COEFFICIENT

As stated previously, the absorption, a, and scattering, b, determine how light propagates over the underwater environment. Both effects are considered in the attenuation coefficient as $c = a + b$, which is usually used to classify the water type [1]. This approach allows us to estimate the attenuation coefficient by using the Beer-Lambert's law as follows

$$c = \frac{-\ln(L_p)}{d} \tag{1}$$

where d is the link distance, and L_p is the propagation loss due to marine particles.

B. SCINTILLATION INDEX

Irradiance fluctuations are measured through the scintillation index, σ^2 given by [26]

$$\sigma^2 = \frac{E[r^2] - E^2[r]}{E^2[r]}, \tag{2}$$

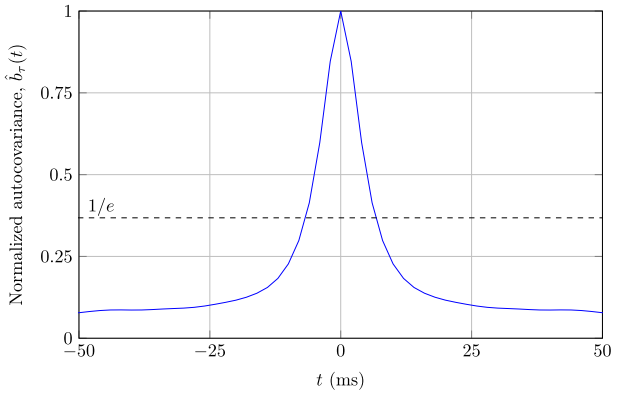

FIGURE 4. Normalized autocovariance of channel fluctuations.

where r is the received signal at the receiver, and $E[\cdot]$ is the expected value.

C. COHERENCE TIME

The coherence time (T_c) measures the period of time over which the fading process is correlated, and may be used for covariance function characterization. The correlation time is related with the normalized temporal covariance function as [27]

$$\hat{b}_\tau(T_c) = \exp(-1), \tag{3}$$

where $\hat{b}_\tau$ is the normalized temporal covariance function given by

$$\hat{b}_\tau(t) = \frac{B_\tau(t)}{B_\tau(0)}, \tag{4}$$

where $B_\tau(t)$ is the temporal covariance function. As an example, in Fig. 4, the normalized temporal autocovariance function and the mentioned threshold in e^{-1} are depicted when small bubbles in tap water are considered.

D. AVERAGE OUTAGE DURATION

According to [28], the average outage duration (AOD) quantifies the average time during which the received signal remains in the outage state. Mathematically, the AOD (in seconds) is given by

$$AOD = \frac{P_{out}}{N}, \tag{5}$$

where P_{out} is the outage probability and N is the frequency of outages at a certain level, defined here as the 10% of the mean received power.

IV. AIR BUBBLES-INDUCED FADING ANALYSIS

In this section, the evaluation metrics discussed above are analyzed when considering an UOWC channel under air bubbles-induced fading with different concentrations of antacid, i.e., different scattering scenarios. Prior to this, it is necessary to study the fluctuations induced by air bubbles in tap water when considering different air bubble sizes. It will serve as a baseline for a comprehensive investigation into the influence of different turbidity levels on the scintillation effects caused by air bubbles and the rest of the evaluation metrics. Furthermore, we analytically model the optical fluctuations under different turbid waters with the generalized Gamma distribution and a mixture of two generalized Gamma distributions.

A. CHANNEL MEASUREMENTS AND CALIBRATION

Before conducting the experimental measurements presented here, an in-depth calibration process was conducted for both the bubble generation device (the air pump) and the antacid solutions utilized to modify the water turbidity. This procedure ensured the consistency of the random behavior of air bubbles across various time moments, leading to a consistent scintillation index for a given air bubble population. Likewise, it was confirmed that the turbidity level, as indicated by the attenuation coefficient for a specific concentration of Maalox per liter, remains reproducible across different time instants.

After the calibration process, channel fluctuations are captured at a sampling rate of 25 kHz at 14 bits resolution for 5 minutes. Then, the collected samples are analyzed in Matlab, where the received optical power is calculated and normalized to the mean of the received optical power in order to obtain the UOWC channel statistics. Finally, histograms and the fitted distributions are also obtained with the help of Matlab.

B. MEASUREMENTS IN TAP WATER

As mentioned in Section II, the irradiance fluctuations due to air bubbles, h_b, are obtained after normalizing the received signal to the mean of the received optical power. In Fig. 5, the histograms of the received optical power fluctuations caused by the stochastic behavior of small and large bubbles with low and high density at link distances of 3 meters in tap water, i.e., no antacid, are represented. These experimental findings demonstrate that the formation of air bubble clusters in a UOWC link leads to significant fluctuations. From Fig. 5, it can be also inferred that the density of air bubbles is a key parameter in the UOWC channel. These preliminary results are in line with previous studies: as the bigger air bubbles population, the stronger intensity fluctuations, both in small and large air bubbles. Additionally, the light blockage, i.e., bins nearby 0, also becomes more pronounced when the density of the bubbles cluster is getting bigger. However, the behavior of these fluctuations depends mainly on the size of the bubbles. On the one hand, fluctuations produced by small bubbles, as depicted in Fig. 5(a), exhibit a behavior similar to those induced by oceanic turbulence, showing fluctuations around the average received power [16]. On the other hand, Fig. 5(b) illustrates how large bubbles-induced fading also manifest a blockage component, which describes the partial or total obstruction of the transmitted optical beam. These findings are also discernible by analyzing the footprints at the receiver plane. Fig. 6(a) illustrates the optical wavefront distortions induced by small bubbles, whereas Fig. 6(a) shows

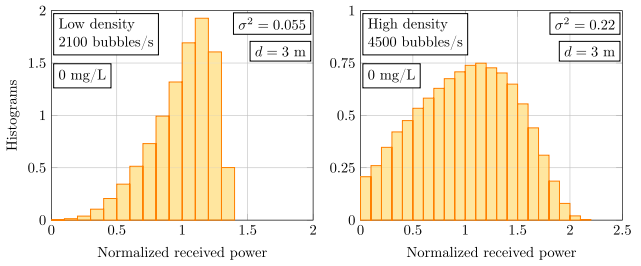

(a) Small air bubbles

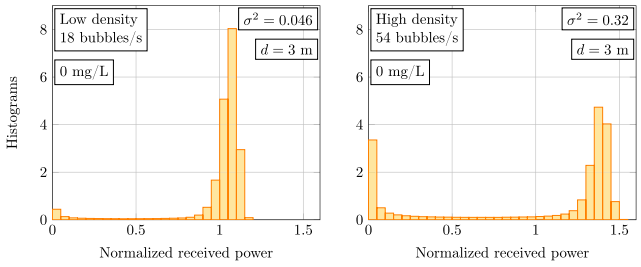

(b) Large air bubbles

FIGURE 5. Histograms of channel fluctuations due to (a) small and (b) large air bubbles.

the blockage of the transmitted optical beam caused by large bubbles.

As can be observed in Table 1, an attenuation coefficient of 0.16 m^{-1} is obtained without air bubbles, which indicates that the tap water is similar to clear ocean water, as well as to the Jerlov IB water type [1], [7]. Secondly, as can be seen in the AOD results, air bubbles produce light blockages of milliseconds on average, which can result in the loss of thousands of consecutive bits for high-data rates UOWC links operating in the order of Mbits/s, especially in the case of large bubbles. Finally, as expected, a slight difference exists in the coherence time between small and large bubbles, where small bubbles exhibit a slightly lower T_c. While previous studies have analyzed the T_c in UOWC channel under oceanic turbulence [16], our findings extend previous reports. We illustrates for the first time that the UOWC channel, exclusively under bubbles-induced scattering, represents a slow-fading channel model for both small and large bubbles since T_c are greater than 1 millisecond for both cases. For the sake of illustration, Fig. 7 show the captured channel fluctuations at different time scales caused by the stochastic behavior of small bubbles with high density at a link distance of 3 meters in tap water. As can be observed, on a timescale of less than milliseconds, the received signal remains constant, indicating the slow-fading nature of fluctuations induced by air bubbles.

C. LOSSES ANALYSIS

As concluded above, the statistical behavior of both small and large bubbles differs qualitatively and quantitatively, as evidenced by the evaluation metrics. Therefore, understanding the impact of air bubbles in terms of propagation losses in the UOWC link for the two analyzed bubble

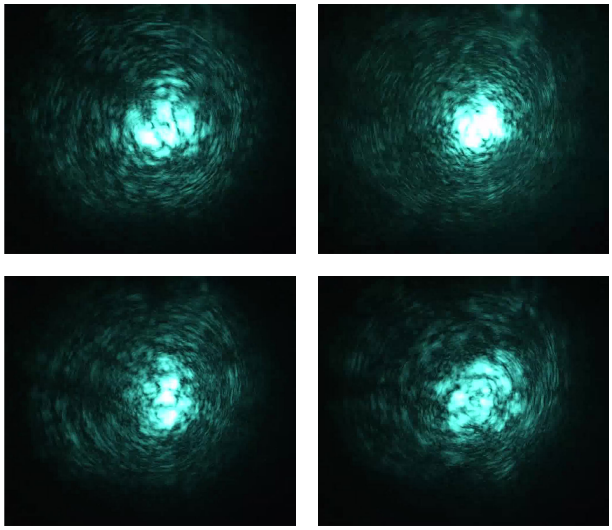

(a) Small air bubbles

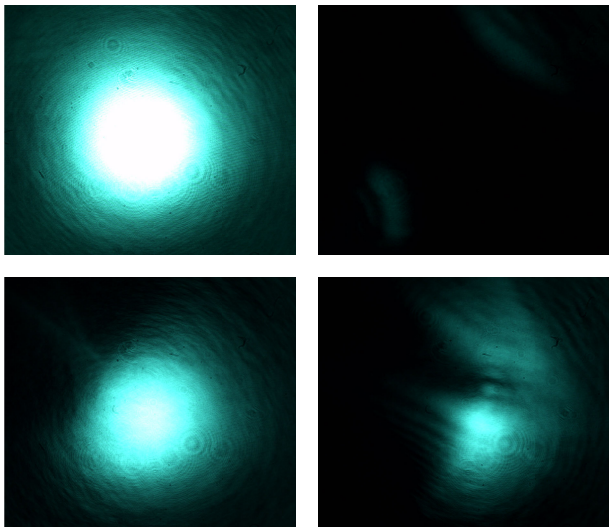

(b) Large air bubbles

FIGURE 6. Received footprints: (a) small bubbles, and (b) large bubbles in high density scenarios.

TABLE 1. Experiment results of the losses due to particles, attenuation coefficient, losses due to air bubbles, AOD and coherence time of the histograms in high density scenarios of small and large bubbles in Fig. 5(a) and Fig. 5(b), respectively.

Channel	L_p (dB)	c (m^{-1})	L_b (dB)	AOD (ms)	T_c (ms)
No bubbles	2.1	0.16	-	-	-
Fig. 5(a)	2.1	0.16	4.7	2.04	6.7
Fig. 5(b)	2.1	0.16	2.9	9.54	11.1

sizes is necessary before characterizing and analyzing the received optical power fluctuations under various turbidity levels. In Fig. 8, the received voltage when tap water and tap water in the presence of small and large air bubbles is represented. It should be noted that the received voltage is obtained after compensate the responsivity of the photodiode, $R = 0.25$ A/W when a wavelength of 520 nm according to their datasheets. The reflectance of the dielectric mirror and the transmission coefficient of the plano-convex lens

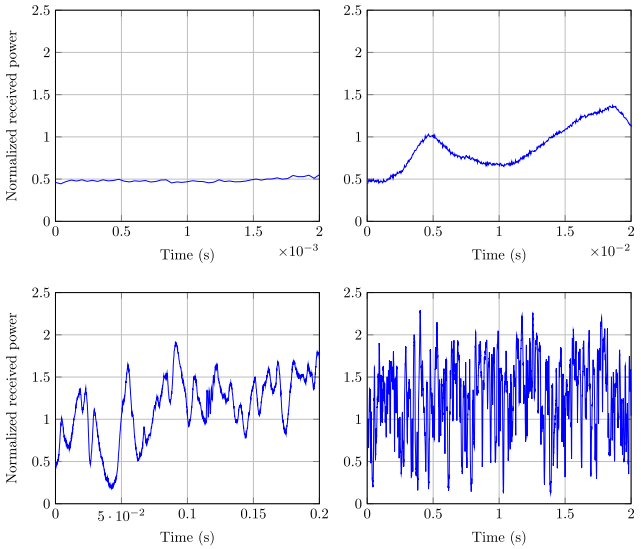

FIGURE 7. Normalized power fluctuations exclusively due to small air bubbles at different time scales.

can be assumed as the unity. As can be observed, the mean value of the received voltage drastically drops in the scenario with bubbles, indicating the presence of losses attributable solely to air bubbles. Furthermore, as can be observed in Fig. 8, losses due to small and large air bubbles present different behavior. For this reason, it is necessary to isolate the losses due to air bubbles, L_b, from the losses due to in-suspension particles, L_p. For this purpose, a measurement is conducted without air bubbles to estimate L_p. Then, the attenuation coefficient can be estimated by using the Eq. (1). Subsequently, the exact measurement is performed in the presence of air bubbles, and hence the total losses, L_T, is estimated from the mean value of the received optical power. Therefore, losses attributable to air bubbles can be isolated based on the measurement of total losses by subtracting the loss due to exclusively in-suspension particles as follows

$$L_b[dB] = L_T[dB] - L_p[dB]. \tag{6}$$

In Table 1, we also present the losses attributable to particles as well as the losses attributable to air bubbles in the measurements of the respective histograms depicted Fig. 5. Our experimental results are consistent with simulation results obtained in [20], which conclude that small bubbles make the propagation losses greater than large bubbles.

D. GENERALIZED GAMMA FITTING

As mentioned in the Introduction, one of the best statistical distributions to model the behavior of experimental measurements in relation to the goodness of fit is the generalized Gamma (Γ_G) as follows [16]

$$\Gamma_G(h_b; a, d, p) = \frac{p}{a^d \Gamma(d/p)} h_b^{d-1} e^{-(h_b/a)^p}, \tag{7}$$

where $\Gamma(\cdot)$ is the Gamma function, a is the scale parameter, d and p are the shape parameters. Given the bimodal behavior

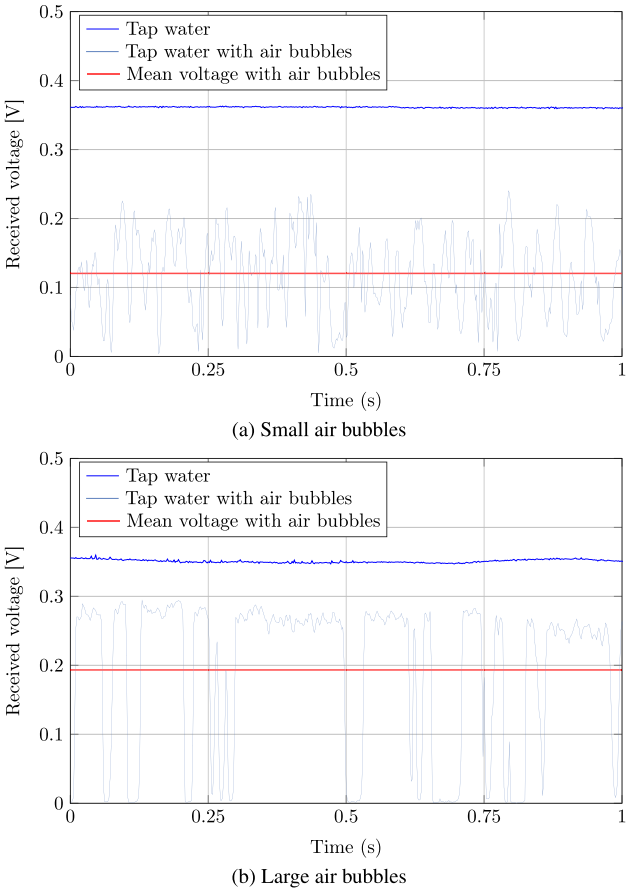

(a) Small air bubbles

(b) Large air bubbles

FIGURE 8. Received voltage when tap water and tap water with (a) small air bubbles and (b) large air bubbles are considered.

exhibited by large air bubbles, we propose for the first time the use of a mixture distribution whose PDF is given as a sum of two Γ_G distributions as follows

$$\begin{aligned}\Gamma_G\Gamma_G(h_b) = w_1\Gamma_G(h_b; a_1, d_1, p_1) \\ + w_2\Gamma_G(h_b; a_2, d_2, p_2),\end{aligned} \tag{8}$$

where w_1 and w_2 are the weights of the blockage and the fluctuation components, respectively. Hence, we model the probability of total or partial blockage due to large bubbles and power fluctuations resulting from particles, wind-generated currents, and small bubbles that are formed through the collision of large bubbles.

E. IMPACT OF WATER TURBIDITY

Figs. 9 and 10 illustrate the impact of particle-induced scattering on the received optical power for different concentrations of antacid solution, considering small and large air bubbles, respectively. As detailed Tables 2 and 3, both proposed models accurately show good fit with the measured data of small and large air bubbles with a coefficient of determination R^2 above 0.95 for all the considered scattering conditions. As expected, the path loss due to marine particles, L_p, increases quickly with the addition of the antacid. It should be noted that the presented scenarios cover a wide range of water

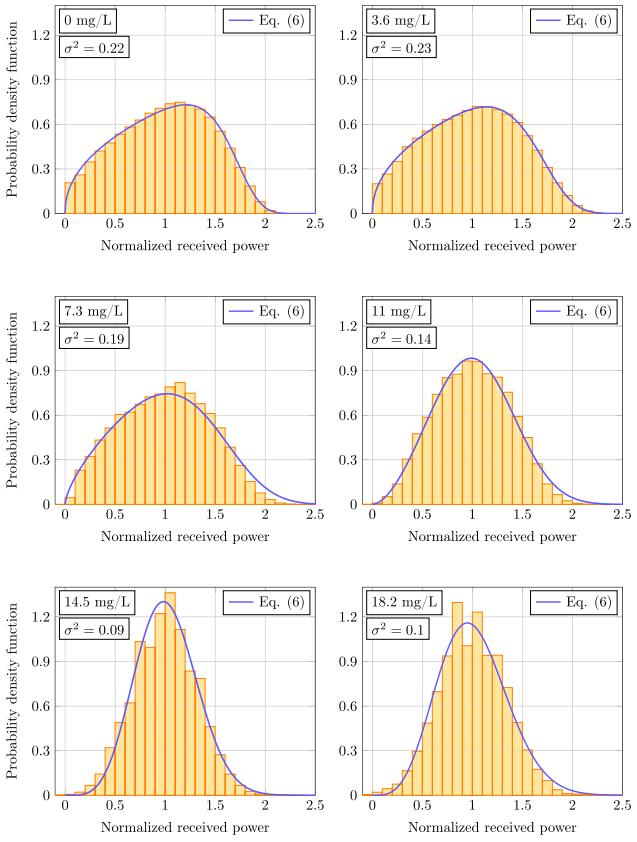

FIGURE 9. Statistical distribution model fitting under different levels of water turbidity when small air bubbles are considered.

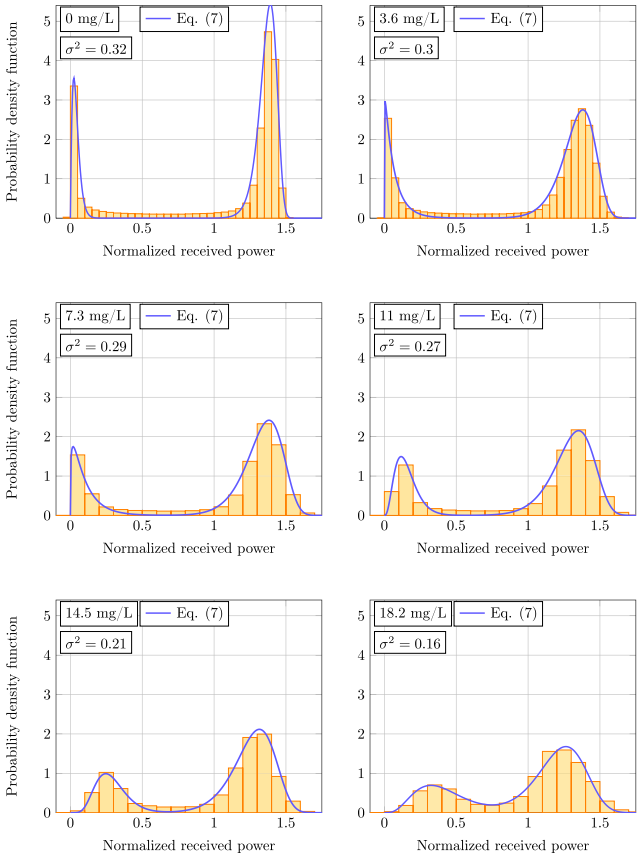

FIGURE 10. Statistical distribution model fitting under different levels of water turbidity when large air bubbles are considered.

types in terms of attenuation. Specifically, the emulated water environments cover from the Jerlov IB to the Jerlov 5C water type when a wavelength of 520 nm is considered [7].

Furthermore, our results go beyond the current literature, as we have demonstrated for the first time that the scintillation index decreases with increasing water turbidity, as can be observed in Fig. 11 in both air bubble sizes. In addition, it is worth noting that the probability of blockage is dramatically reduced when increasing the antacid concentration per liter in the water tank. While this effect is observed in both sizes of air bubbles, it is particularly pronounced in larger bubbles, as depicted in Fig. 10. Physically, it appears that the fluctuations caused by air bubbles can be mitigated through a more significant collection of scattered photons resulting from the particle-induced scattering effect. Moreover, it is well known that increasing the level of scattering results in greater beamwidth broadening due to propagation through a more dispersive medium [29]. This results in a smaller relative size of the air bubble compared to the beam width, thereby reducing the likelihood of blockage. Therefore, while higher geometric and propagation losses are incurred as the antacid concentration, i.e., the turbidity levels, increases, a higher robustness to air bubble fading is achieved due to the beam expansion. This effect could similarly be achieved by employing UOWC systems with LD sources that have a larger

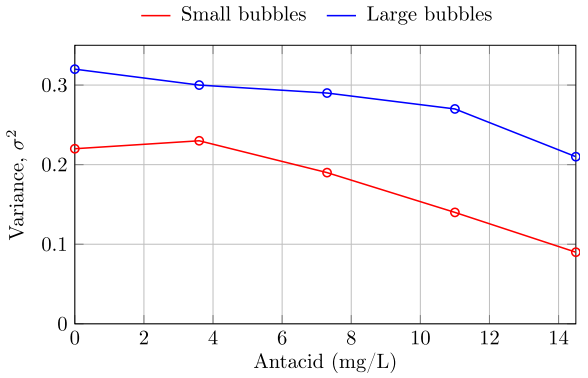

FIGURE 11. Scintillation index of small and large air bubbles under different levels of water turbidity.

beam width, as well as utilizing lenses with larger diameters at the receiver.

In line with the decrease in light blockage, the AOD represented in Fig. 12(a) is also significantly reduced due to water turbidity in both air bubbles cases. Most notably, this study presents compelling evidence for mitigating light blockage caused by air bubbles, thanks to the particle-induced scattering effect. Nevertheless, as depicted in Fig. 12(b), the coherence time remains constant for all the considered amounts of antacid, both small and large air bubbles. Thus, it can be concluded that water turbidity has no impact on the

TABLE 2. Experiment results of losses due to particles, attenuation coefficient, losses due to air bubbles, fitting parameters for generalized Gamma and R^2 of the histograms in Fig. 9.

Antacid [mg/L]	L_p [dB]	c [m^{-1}]	L_b [dB]	$\Gamma_G(a,d,p)$	R^2
0	2.1	0.16	4.7	(1.73, 1.43, 7.95)	0.99
3.6	7	0.54	4.7	(1.72, 1.44, 6.28)	0.99
7.3	10	0.77	4.7	(1.59, 1.68, 4)	0.98
11	12.7	0.98	4.7	(1.19, 2.75, 3.05)	0.99
14.5	16.2	1.24	4.7	(0.79, 5.09, 2.41)	0.98
18.2	17.7	1.36	4.7	(0.75, 4.45, 2.1)	0.99

TABLE 3. Experiment results of losses due to particles, attenuation coefficient, losses due to air bubbles, fitting parameters for the mixture of generalized Gamma and R^2 of the histograms in Fig. 10.

Antacid [mg/L]	L_p [dB]	c [m^{-1}]	L_b [dB]	$\Gamma_G(a_1,d_1,p_1)$	w_1	$\Gamma_G(a_2,d_2,p_2)$	w_2	R^2
0	2.1	0.16	2.9	(0.028, 2, 1.2)	0.2	(1.38, 29.38, 22.7)	0.8	0.95
3.6	7	0.54	2.9	(0.05, 1.110, 0.85)	0.23	(1.38, 13.95, 12.8)	0.77	0.98
7.3	10	0.77	2.9	(0.06, 1.320, 0.85)	0.23	(1.39, 11.93, 11.7)	0.77	0.98
11	12.7	0.98	2.9	(0.047, 3.77, 1.060)	0.26	(1.36, 10.87, 10.55)	0.74	0.98
14.5	16.2	1.24	2.9	(0.037, 7.28, 0.98)	0.25	(1.33, 10.87, 10.2)	0.75	0.98
18.2	17.7	1.36	2.9	(0.09, 4.57, 1.03)	0.3	(1.26, 8.92, 7.65)	0.7	0.98

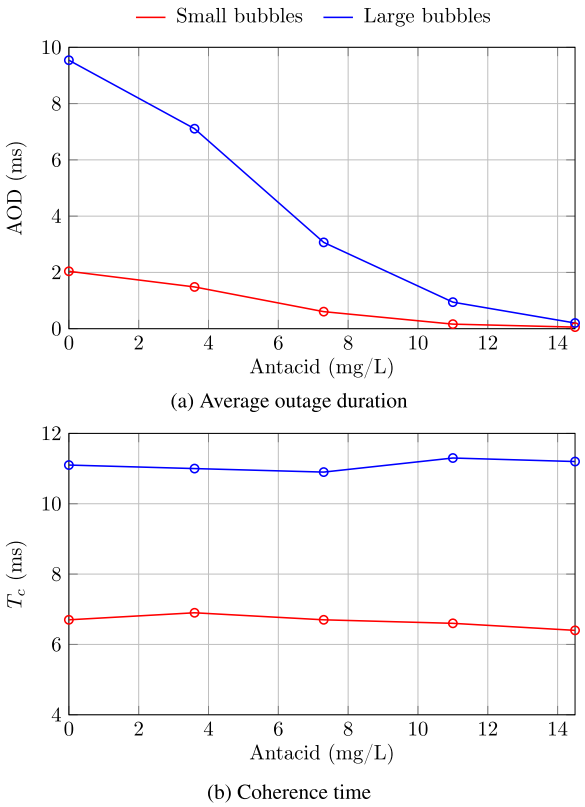

(a) Average outage duration

(b) Coherence time

FIGURE 12. (a) Average outage duration and (b) coherence time of small and large air bubbles under different levels of water turbidity.

temporal correlation of UOWC channels under air bubbles-induced fading. As far as we know, these findings have not been presented yet in the context of experimental UOWC channel characterization. Our current research contributes to the existing understanding of the impact of particle-induced scattering in UOWC systems affected by random variations in the refractive index due to air bubbles or oceanic turbulence [6], [30]. Consequently, our experiments can be used to accurately model natural waters bodies by considering the relationship between air bubbles and water turbidity.

V. CONCLUSION

In conclusion, this work provides a comprehensive analysis and characterization of the UOWC channel based on experimental measurements, focusing on the influence of the air bubbles size and the water turbidity. The presented results shed light on the different behaviors exhibited by small and large bubbles in terms of fading effect and obstruction of light. Unlike previous studies of air bubbles in UOWC channels have overlooked the scattering phenomenon, this work provides UOWC system designers with valuable insights for efficiently adapting future designs of advanced UOWC transceivers to realistic ocean conditions. Specifically, our experimental findings indicate that despite the high attenuation produced by the scattering, it can also reduce the fluctuations caused by air bubbles, by mitigating the partial or total light blockage. The scintillation index and the AOD are significantly lowered when the antacid concentration increases. These novel insights about the underwater channel offers UOWC system designers valuable insights to adeptly future UOWC systems designs for enhanced efficiency in turbid maritime environments in presence of air bubbles.

This research could be extended by thoroughly examining the influence of additional link parameters, such as transmission distance, on the fitted parameters of the proposed distribution and the probability of blockage. Future work should also include an experimental UOWC system in

order to evaluate the BER performance under the proposed channel model with different turbid scenarios. Additionally, the water tank could be filled with different real water samples to validate the channel model comprehensively. Lastly, the proposed theoretical channel model could be enhanced by incorporating the impact of link misalignment of optical transceivers and light scintillation caused by oceanic turbulence.

REFERENCES

[1] Z. Zeng, S. Fu, H. Zhang, Y. Dong, and J. Cheng, "A survey of underwater optical wireless communications," *IEEE Commun. Surveys Tuts.*, vol. 19, no. 1, pp. 204–238, 1st Quart., 2017.

[2] X. Sun, C. H. Kang, M. Kong, O. Alkhazragi, Y. Guo, M. Ouhssain, Y. Weng, B. H. Jones, T. K. Ng, and B. S. Ooi, "A review on practical considerations and solutions in underwater wireless optical communication," *J. Lightw. Technol.*, vol. 38, no. 2, pp. 421–431, Jan. 2020.

[3] A. Immas and M.-R. Alam, "Guidance, navigation, and control of AUVs for permanent underwater optical networks," *IEEE J. Ocean. Eng.*, vol. 48, no. 1, pp. 43–58, Jan. 2023.

[4] B. Cochenour, L. Mullen, and J. Muth, "Temporal response of the underwater optical channel for high-bandwidth wireless laser communications," *IEEE J. Ocean. Eng.*, vol. 38, no. 4, pp. 730–742, Oct. 2013.

[5] R. Boluda-Ruiz, P. Rico-Pinazo, B. Castillo-Vázquez, A. García-Zambrana, and K. Qaraqe, "Impulse response modeling of underwater optical scattering channels for wireless communication," *IEEE Photon. J.*, vol. 12, no. 4, pp. 1–14, Aug. 2020.

[6] R. Boluda-Ruiz, P. Salcedo-Serrano, B. Castillo-Vázquez, A. García-Zambrana, and J. M. Garrido-Balsells, "Impact of scattering on secrecy outage probability of underwater optical wireless links," *IEEE J. Ocean. Eng.*, vol. 48, no. 4, pp. 1362–1372, Oct. 2023.

[7] C. A. Williamson and R. C. Hollins, "Measured IOPs of Jerlov water types," *Appl. Opt.*, vol. 61, no. 33, pp. 9951–9961, Nov. 2022.

[8] H. M. Oubei, E. Zedini, R. T. ElAfandy, A. Kammoun, T. K. Ng, M.-S. Alouini, and B. S. Ooi, "Efficient Weibull channel model for salinity induced turbulent underwater wireless optical communications," in *Proc. Opto-Electronics Commun. Conf. (OECC) Photon. Global Conf. (PGC)*, Jul. 2017, pp. 1–2.

[9] Z. Vali, A. Gholami, Z. Ghassemlooy, M. Omoomi, and D. G. Michelson, "Experimental study of the turbulence effect on underwater optical wireless communications," *Appl. Opt.*, vol. 57, no. 28, pp. 8314–8319, Oct. 2018.

[10] X. Zhang, M. Lewis, and B. Johnson, "Influence of bubbles on scattering of light in the ocean," *Appl. Opt.*, vol. 37, no. 27, pp. 6525–6536, Sep. 1998.

[11] S. Thorpe, "Bubble clouds and the dynamics of the upper ocean," *Quart. J. Roy. Meteorological Soc.*, vol. 118, no. 503, pp. 1–22, Jan. 1992.

[12] S. Vahaji, L. Chen, S. C. P. Cheung, and J. Tu, "Numerical investigation on bubble size distribution around an underwater vehicle," *Appl. Ocean Res.*, vol. 78, pp. 254–266, Sep. 2018.

[13] J. R. Waaland and D. Branton, "Gas vacuole development in a blue-green alga," *Science*, vol. 163, no. 3873, pp. 1339–1341, Mar. 1969.

[14] S. Ling and H. Pao, "Study of micro-bubbles in the north sea," in *Sea Surface Sound: Natural Mechanisms of Surface Generated Noise in the Ocean*. Berlin, Germany: Springer, 1988, pp. 197–210.

[15] H. M. Oubei, R. T. ElAfandy, K.-H. Park, T. K. Ng, M.-S. Alouini, and B. S. Ooi, "Performance evaluation of underwater wireless optical communications links in the presence of different air bubble populations," *IEEE Photon. J.*, vol. 9, no. 2, pp. 1–9, Apr. 2017.

[16] M. V. Jamali, A. Mirani, A. Parsay, B. Abolhassani, P. Nabavi, A. Chizari, P. Khorramshahi, S. Abdollahramezani, and J. A. Salehi, "Statistical studies of fading in underwater wireless optical channels in the presence of air bubble, temperature, and salinity random variations," *IEEE Trans. Commun.*, vol. 66, no. 10, pp. 4706–4723, Oct. 2018.

[17] E. Zedini, H. M. Oubei, A. Kammoun, M. Hamdi, B. S. Ooi, and M.-S. Alouini, "Unified statistical channel model for turbulence-induced fading in underwater wireless optical communication systems," *IEEE Trans. Commun.*, vol. 67, no. 4, pp. 2893–2907, Apr. 2019.

[18] D. Chen, J. Wang, S. Li, and Z. Xu, "Effects of air bubbles on underwater optical wireless communication [invited]," *Chin. Opt. Lett.*, vol. 17, no. 10, 2019, Art. no. 100008.

[19] M. Shin, K.-H. Park, and M.-S. Alouini, "Statistical modeling of the impact of underwater bubbles on an optical wireless channel," *IEEE Open J. Commun. Soc.*, vol. 1, pp. 808–818, 2020.

[20] L. Kou, J. Zhang, P. Zhang, Y. Yang, and F. He, "Composite channel modeling for underwater optical wireless communication and analysis of multiple scattering characteristics," *Opt. Exp.*, vol. 31, no. 7, pp. 11320–11334, Mar. 2023.

[21] *The Sonardyne Site: BlueComm Underwater Optical Communications*. Sonardyne International. [Online]. Available: http://www.sonardyne.com/

[22] *LUMA: Fast Underwater Wireless Communication*. [Online]. Available: https://www.hydromea.com/underwater-wireless-communication/

[23] L. Mullen, D. Alley, and B. Cochenour, "Investigation of the effect of scattering agent and scattering albedo on modulated light propagation in water," *Appl. Opt.*, vol. 50, no. 10, pp. 1396–1404, 2011.

[24] A. Laux, R. Billmers, L. Mullen, B. Concannon, J. Davis, J. Prentice, and V. Contarino, "The a, b, c s of oceanographic LiDAR predictions: A significant step toward closing the loop between theory and experiment," *J. Modern Opt.*, vol. 49, nos. 3–4, pp. 439–451, Mar. 2002.

[25] (Jun. 2021). *STEMlab 125-14—Red Pitaya*. [Online]. Available: https://redpitaya.com/stemlab-125-14/

[26] L. C. Andrews and R. L. Phillips, *Laser Beam Propagation Through Random Media*, vol. 1. Bellingham, WA, USA: SPIE, 2005.

[27] A. Mostafa and S. Hranilovic, "Channel measurement and Markov modeling of an urban free-space optical link," *J. Opt. Commun. Netw.*, vol. 4, no. 10, pp. 836–846, Oct. 2012.

[28] M. K. Simon and M.-S. Alouini, *Digital Communications Over Fading Channels*, 2nd ed. Hoboken, NJ, USA: Wiley, 2005.

[29] R. Boluda-Ruiz, A. García-Zambrana, B. Castillo-Vázquez, and S. Hranilovic, "Impact of angular pointing error on BER performance of underwater optical wireless links," *Opt. Exp.*, vol. 28, no. 23, pp. 34606–34622, 2020.

[30] P. Salcedo-Serrano, R. Boluda-Ruiz, J. M. Garrido-Balsells, and A. García-Zambrana, "On the scattering-induced fading for optical wireless links through seawater: Statistical characterization and its applications," *Opt. Exp.*, vol. 29, no. 23, p. 37101, Nov. 2021.

PEDRO SALCEDO-SERRANO was born in Granada, Spain, in 1997. He received the B.Sc. and M.Sc. degrees in telecommunication engineering (acoustic and communications) from the University of Málaga, Málaga, Spain, in 2019 and 2020, respectively. Since 2021, he has been a Pre-Doctoral Researcher with the Communications Engineering Department, University of Málaga. His current research interests include information theory and its application to design and performance analysis of underwater optical wireless communication systems, with an emphasis on underwater channel modeling.

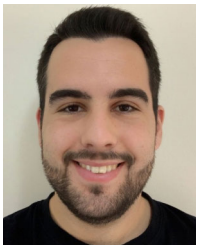

CARLOS GÓMEZ-GARCÍA was born in Córdoba, Spain, in 1998. He received the B.Sc. degree in telecommunication engineering from the University of Málaga, Málaga, Spain, in 2023.

JACQUELINE IAMAGUTI-DEBESSA was born in São Paulo, Brazil, in 2000. She received the B.Sc. degree in telecommunication engineering from the University of Málaga, Málaga, Spain, in 2023.

RUBÉN BOLUDA-RUIZ was born in Málaga, Spain, in 1986. He received the B.Sc. and M.Sc. degrees in telecommunication engineering (electronics and communications), and the Ph.D. degree in electrical engineering from the University of Málaga, Málaga, in 2012, 2014, and 2017, respectively.

From 2010 to 2013, he was a Software Engineer with telecommunication industry. In 2016, he was a Visiting Researcher with the Department of Electrical and Computer Engineering, McMaster University, Hamilton, ON, Canada. From October 2017 to December 2019, he was a Post-Doctoral Research Associate with the Electrical and Computer Engineering Program, Texas A&M University at Qatar. From January 2020 to May 2021, he was a Postdoctoral Researcher with the Communications Engineering Department, University of Málaga, where he has been an Assistant Professor with the Communications Engineering Department, since May 2021. He has authored/coauthored more than 50 journal and conference publications. His current research interests include theory and its application to design and performance analysis of terrestrial and underwater free-space optical (FSO) communication systems, with a current emphasis on channel modeling, multiple-input/multiple-output (MIMO) systems, and physical layer security aspects.

Dr. Boluda-Ruiz was a recipient of the Best Ph.D. Thesis in Electrical Engineering (Extraordinary Doctorate Award) by the University of Málaga (2017–2018); the Best Ph.D. Thesis in Electrical Engineering in the XVI Night of Telecommunications by the Agencia Andaluza de Ingenieros de Telecomunicación (AAIT), in 2018; the TAMUQ Research Excellence Award, in 2018; and the Exemplary Reviewer Certificate of 2021 by IEEE TRANSACTIONS ON COMMUNICATIONS. He is an Active Reviewer of various IEEE and Optica top journals.

JOSÉ MARÍA GARRIDO-BALSELLS was born in Granada, Spain, in 1974. He received the M.S. and Ph.D. degrees in telecommunications engineering from the University of Málaga, Spain, in 1999 and 2008, respectively.

He was a Consultant and the Technical Manager of several telecommunications companies, for three years. In 2001, he joined the Communications Engineering Department, University of Málaga, as a full-time Assistant Professor (LRU), where he is currently an Associate Professor. Since 2020, he has also been with the TELMA Research Institute, University of Málaga. Since 2001, he has been with the TIC-102 Research Group, Regional Government of Andalusia. He has authored or coauthored 70 journal and conference publications and participating actively as a principal investigator in research projects and contracts with national and international companies. His research interests include wireless optical communications, including indoor visual light communications (VLC) and outdoor optical communications systems through turbulent and dispersive media such atmospheric or underwater. He is also interested in topics related to adaptive optics applications, including machine learning control algorithms, structured light, and OAM vortex beams or channel coding schemes.

BEATRIZ CASTILLO-VÁZQUEZ was born in Madrid, Spain, in 1971. She received the M.Sc. and Ph.D. degrees in electrical engineering from the University of Málaga, in 1994 and 1999, respectively. In 1995, she joined the Department of Communications Engineering, University of Málaga, where she currently holds the position of an Associate Professor. Her research interests primarily include optical wireless communications, including free-space optics (FSO), underwater optical wireless communications (UOWC), channel modeling, relay/multihop communications, and physical layer secrecy issues.

ANTONIO PUERTA-NOTARIO received the Telecommunication Engineering degree from the Technical University of Madrid, Spain, in 1973, and the Ph.D. degree in telecommunication engineering from the Technical University of Barcelona, Spain, in 1982. From 1973 to 1989, he was an Associate Professor with the Telecommunication Engineering School, Barcelona, where he has engaged in teaching applied mathematics and circuits theory, research and development for industrial applications, and research on switched capacitor circuits. In 1990, he joined the University of Málaga, Spain, as a Full Professor with the Department of Communications Engineering. Since 1994, he has been the Director of the Telecommunication Engineering School, University of Málaga. His current research interests include optical receivers and transmitter design and wireless optical communications.

ANTONIO GARCÍA-ZAMBRANA was born in Málaga, Spain, in 1970. He received the M.Sc. and Ph.D. degrees in electrical engineering from the University of Málaga, in 1994 and 1998, respectively. Following his education, he joined the Department of Communications Engineering, University of Málaga, in 1994, where he currently holds the position of a Full Professor. He has made significant contributions to the field of optical wireless communications. His research interests primarily revolve around this area, encompassing various aspects, such as free-space optics, underwater optical wireless communications, channel modeling, relay/multihop communications, and physical layer secrecy issues.